RAPID, APPROXIMATE MULTI-AXIS VIBRATION TESTING

Ethan Savoy Cramer, BS

Thesis Prepared for the Degree of

MASTER OF SCIENCE

UNIVERSITY OF NORTH TEXAS

May 2023

APPROVED:

Richard Zhang, Major Professor
Hamid Sadat, Committee Member
Yunwei Xu, Committee Member
Herman Shen, Chair of the Department of Mechanical Engineering
Shengli Fu, Interim Dean of the College of Engineering
Victor Prybutok, Dean of the Toulouse Graduate School

Cramer, Ethan Savoy. *Rapid, Approximate Multi-Axis Vibration Testing*. Master of Science (Mechanical and Energy Engineering), May 2023, 43 pp., 9 tables, 23 figures, 41 numbered references.

Sequential single-axis vibration testing strategies often produce over-testing when qualifying system hardware. Multi-axis excitation techniques can simulate realistic service environments, but the hardware and testing strategies needed to do so tend to be costly and complex. Test engineers instead must execute sequential tests on single-axis shaker tables to excite each degree of freedom, which the previous two decades of vibration testing literature have shown to cause extensive over-testing when considering cross-axis responses in assessing the severity of the applied test environments. Traditional assessments assume that the test article responds only in the axis of excitation, but often significant response occurs in the off-axes as well. This paper proposes a method to address the over-testing problem by approximating a simultaneous multi-axis test using readily-available, single-axis shaker tables. By optimizing the angle of excitation and the boundary condition through dynamic test fixture design, the test article can be tested using a Single-Input, Multiple-Output (SIMO) test in a way that approximates a Multiple-Input, Multiple-Output (MIMO) test. This paper shows the proposed method in simulation with a 2D finite element box assembly with removable component (BARC) model attached to springs with variable stiffness. The results include quantified test quality assessment metrics with comparison to standard sequential testing. The proposed method enables access to rapid, approximate, multi-axis testing using existing hardware, thereby reducing the over-conservatism of sequential single-axis tests and requisite over-design of systems.

ACKNOWLEDGEMENTS

This thesis is reproduced from Cramer, E., Harvey, D., & Zhang, R. (2023), IMAC-XLI, in Proceedings of the 2023 Annual Conference on Experimental and Applied Mechanics (Ser. Conference Proceedings of the Society for Experimental Mechanics Series), Baar, Zug, Switzerland, with permission from the Society for Experimental Mechanics, Inc.

I would like to thank my mentor, Dustin Harvey, and my advisor, Richard Zhang. Dustin has provided invaluable encouragement, guidance, and insight during my post-baccalaureate year at Los Alamos National Lab as well as during my graduate studies. Dustin is incredibly bright, but also modest and patient, a rare combination of traits. I could not be more grateful for his mentorship. I would be no where near the engineer that I am today without it. Dr. Zhang has also been a consistent source of encouragement throughout my academic career. I would not have gone onto graduate school without the year I spent in his research lab, nor would I have ever applied to work at Los Alamos National Lab. It's safe to say that this thesis would not exist were it not for his push.

I want to thank my wife, Ryleigh. She has been the best friend one could hope for and seeing her complete her graduate studies a semester ahead of my own provided me with the perseverance I needed to make it to the end. I also want to thank my family—my mother, father, and brother. They've always been supportive of all my endeavors. They also provided me with a willing (or captive) audience to bounce ideas off of and explain tricky concepts. I appreciate so much how curious they were about the work that I was doing.

TABLE OF CONTENTS

Page

LIST OF TABLES

Page

LIST OF FIGURES

Page

INTRODUCTION

The aerospace industry uses vibration shaker tables to perform component durability testing. In these tests a component, piece of equipment, or entire system is attached to a shaker table where it is subjected to dynamic excitation. The goal is to understand how the article under test will perform in its service environment without having to run it through its entire service life via field testing.

In a vibration test, an aerospace system or component is qualified if it is shown to survive a test meant to replicate its lifetime service conditions. The test is designed based on recorded field data. To develop a test, a system is taken through all of its intended environments, e.g., transportation, launch, and reentry. Acceleration data measured from these environments is then brought back to the lab and imported into a shaker table controller. The controller then drives a vibration test intended to mimic the acceleration conditions experienced by the system or specific components of the system in the field. However, it is often difficult to match the measured field response in a lab test. This is largely due to the test's boundary conditions and excitation methods.

In a lab test, a shaker table is the excitation source. The two most common shaker table types, differentiated by their number of independent degrees of freedom, are single-axis and multi-axis shaker tables. Multi-axis shakers have the ability to reproduce service environments more realistically, as real accelerations inevitably produce multiple degrees of freedom of excitation simultaneously. Figure 1 depicts a generic multi-axis testing setup on a three-axis shaker table. Often multi-axis tests use six-degree-of-freedom (6DOF) shaker tables. Yet multi-axis shakers are not yet common in the aerospace industry due in part to their high cost and the difficulty for

shaker controllers to handle the added complexity. Single-axis shaker tables are much more common. They are not as expensive to purchase and have a wide range of control software options.

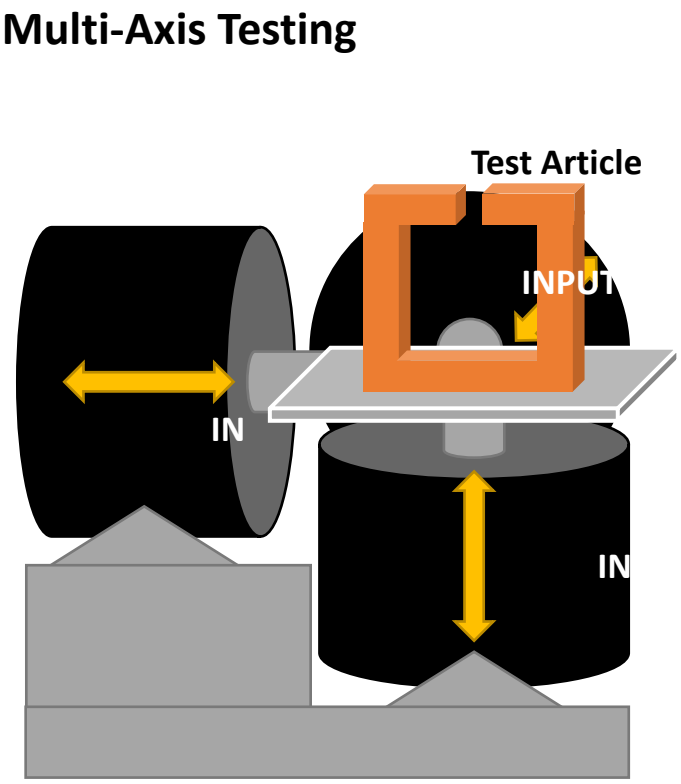

Figure 1: Diagram of a generic multi-axis vibration test setup.

In an ideal test, the component would be run through its required accelerations in real time using a six degree of freedom shaker table, but this is not often possible. These tests are typically constrained by cost, complexity, and duration. Aerospace laboratories employ standard test strategies that need to work for test articles of varying size, complexity, and intended lifetime. Therefore, a general strategy must be devised to test multiple degrees of freedom using single-axis shaker tables. This is usually accomplished by running three sequential tests, one in each of the component's primary axes. A typical sequential single-axis test sequence is shown in Figure 2. The result is

assumed to be equivalent to a simultaneous multi-axis test, but in practice this is rarely the case.

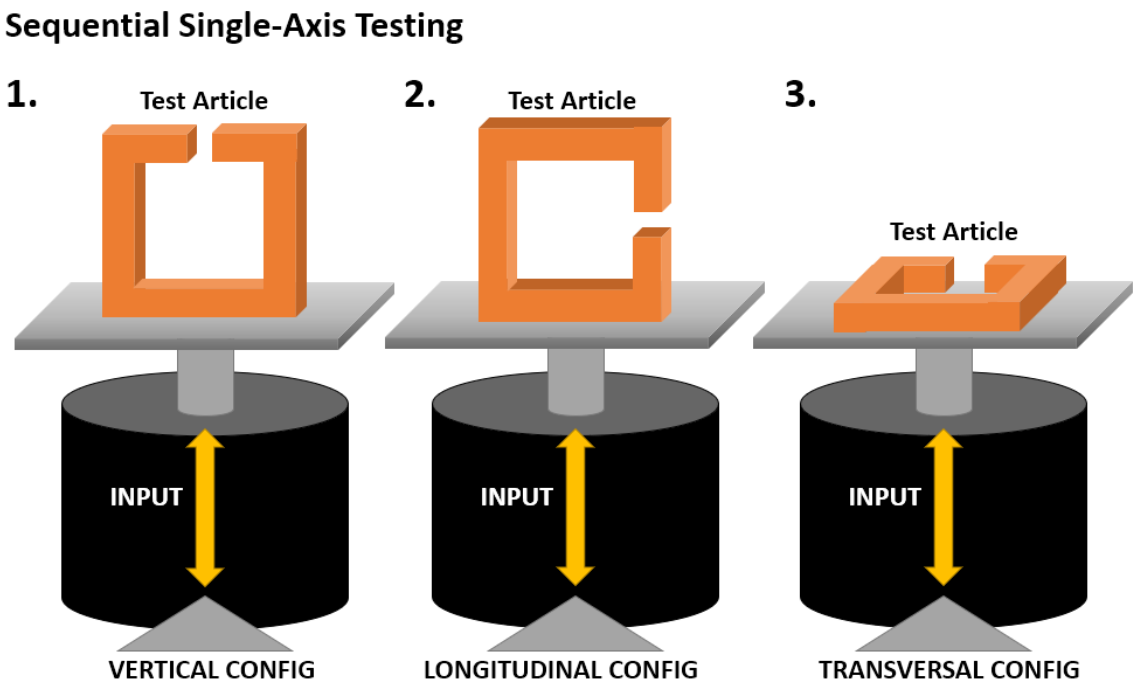

Figure 2: Diagram of a sequential single-axis vibration test setup.

This assumption, that three sequential single-axis tests is equivalent to a multi-axis test, neglects the cross-axis responses that occur in axes other than the primary axis. A single-axis test designed to excite the X-axis of a component may well produce significant response in the component's Y-axis and Z-axis. That component will then be tested two more times, resulting in three full duration responses in all three primary axes when the goal had been to excite one full duration response in each axis. This is clearly over-testing, though the degree of over-testing varies with the amplitude of the cross-axis response. Over-testing causes unnecessary costs in strengthening the design and may result in designs that do not accurately account for the service environment. Recent work has confirmed that there is usually a substantial increase in test severity

when cross-axis responses are considered (Bouma et al., 2019).

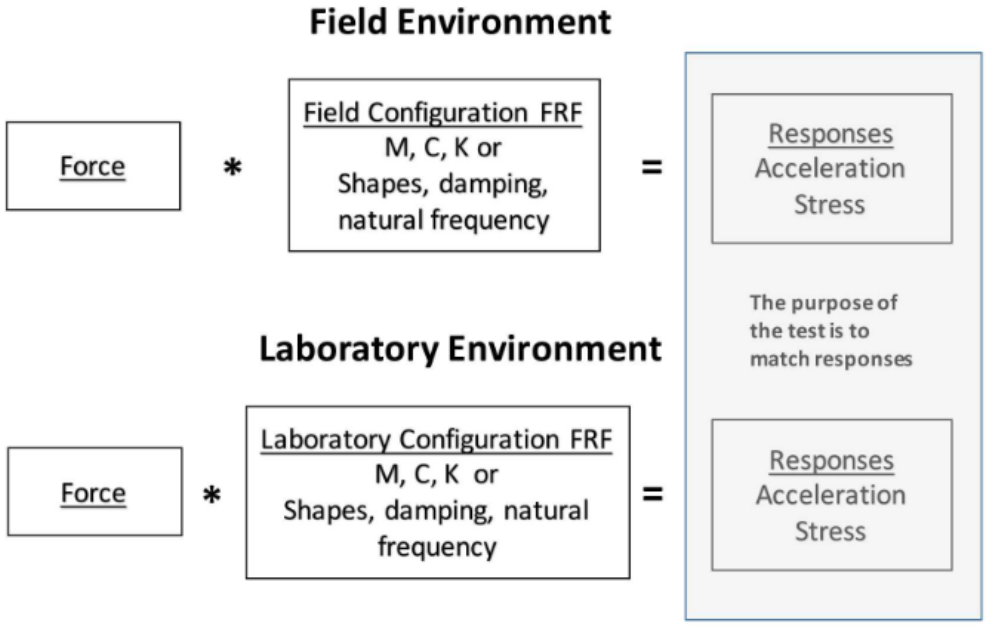

Figure 3: The purpose of dynamic environments testing is to match the field responses in a laboratory test (Schoenherr et al., 2020).

Another critical aspect of qualification test design is the boundary condition. In a lab test, the boundary condition is defined by the test fixture. The test fixture attaches the component to the shaker table. Test fixture design is usually approached from a cost, schedule, and safety perspective, while the question of whether or not the fixture improves test quality often remains unconsidered. These fixtures are typically rigid in order to minimize cross-axis responses, though even a rigid fixture cannot entirely prevent them. Rigid fixtures are used to ensure that the fixture resonances and test article dynamics avoid coupling. Rigid fixtures have problems, though. They do not usually represent the impedance of the service environment's attachment condition which causes a boundary condition mismatch. Qualification tests attempt to match the test article's acceleration and stress response to those experienced in the service

environment. Figure 3 visualizes the desired outcome. When using a rigid fixture, or any fixture not designed to replicate the service environment boundary conditions, it is difficult or impossible to provide a shaker table input that can mimic the service environment responses.

Published work that attempts to understand the difficulty of replicating field environments in the lab began in the 1960s, in the Apollo era, when huge advances in component qualification testing were made. One early paper presents theoretical methods for quantifying the mechanical impedance of a multi-degree of freedom system, and how that system responds when excited (On, 1967). A following work builds upon On's impedance matrix formulations to develop vibration test fixtures that simulate the mount impedance of aerospace structures (Scharton, 1969). Scharton found that a rigid fixture causes unrealistically high vibration transfer functions from the fixture into the component, because rigid fixtures do not simulate the mounting impedance of the component in the field. He writes, "if the multimodal fixture testing concept is employed, a single test can be conducted at high frequencies and the vibration environment on the spacecraft will simultaneously simulate the environment generated in conventional tests conducted along each of three perpendicular axes. Vibration tests utilizing the multimodal test fixture concept will generally result in a more triaxial spacecraft vibration environment in the high-frequency regime than tests performed with conventional fixtures excited along a single axis." (Scharton, 1969). In this quote, the term conventional fixtures means rigid fixtures, which are designed such that the test never excites them anywhere near their resonant frequency. Multimodal

test fixtures are therefore fixtures designed to operate in the vicinity of their first few resonant frequencies.

Some of Scharton's concerns have been solved using multi-axis excitation methods (i.e., 6DOF shaker tables). Researchers have conducted various comparisons of single-axis and multi-axis vibration tests. Researchers found that not only do sequential single-axis tests lead to undue stress, but they also lead to entirely different failure times, failure distributions, and failure modes (French et al., 2006). This implies that a sequential single-axis test is not only more severe than it needs to be, but the failure it induces is not even the same failure as induced by a multi-axis test. A later study tested a more complex part with both single-axis and 6DOF excitation methods and validated both tests with finite element models (Gregory et al., 2009). They found that the magnitude and location of the maximum Von Mises stress were different for both excitation methods, and that modal participations were different as well.

Despite a large body of evidence, sequential single-axis testing remains the status-quo in aerospace qualification testing. This is largely driven by economics. Even though 6DOF shaker tables are able to better reproduce the service environment (French et al., 2006), they are prohibitively costly and often not a feasible option for large systems-level tests. A near-term solution must employ single-axis shakers.

Within these limitations, many strategies have emerged to address the difficulties in simulating an intended field environment. Two broad categories of approaches have appeared to address the mismatch between field environments and test setups: impedance modification approaches, and input control approaches (Jones et al., 2018).

Impedance modification, broadly, means test fixture design. These methods attempt to design a fixture which accounts for the impedance experienced by the component in the field. Scharton's multimodal test fixtures fit into this category. Another method is "N+1" fixtures, which uses a fixture that simulates the service environment impedance by using a part of the service environment structure as the test fixture (Hall, 2020). For example, if a component is attached to an aluminum L-bracket in the field, then that aluminum L-bracket is used as the laboratory test fixture.

Another form of impedance modification is using topological optimization to design a test fixture. A recent work that used topological optimization to design an impedance matched test fixture found the design problem intractable due to the high number of local minima in the solution space (Schoenherr, 2020). This study used the mismatch between laboratory and field frequency response functions as the objective function, but that objective function was non-convex and had many local minima. This thesis presents an impedance modification approach similar to the topological optimization study, but our proposed method seeks to avoid the local minima problem by using a smaller design space and a lower dimensional finite element model (2D instead of 3D).

One of the most productive branches of impedance modification research is Impedance-Matched Multi Axis Testing (IMMAT). This method uses multiple single-axis shakers simultaneously to apply distributed force inputs. A comparison of IMMAT and sequential single-axis testing found that IMMAT has enhanced replication of the service environment, shorter test durations, and a significant reduction in costs associated with random vibration tests (Daborn et al., 2014).

Input control approaches seek to mimic the field environment by changing how the test article is excited. One such modeling based approach utilizes dynamic substructuring to determine better excitation strategies by decoupling a system into the fixed-base modes of the test article and test fixture. This method allows one to understand only the damaging energy experienced by the component while ignoring the rigid body motion of the fixture. These decoupled modes can be analyzed to understand whether the test setup is adequately capturing the damage mechanisms of the service environment; if it is not, the analysis can reveal how to properly excite the test fixture in order to activate those damaging modes (Harvie, 2017).

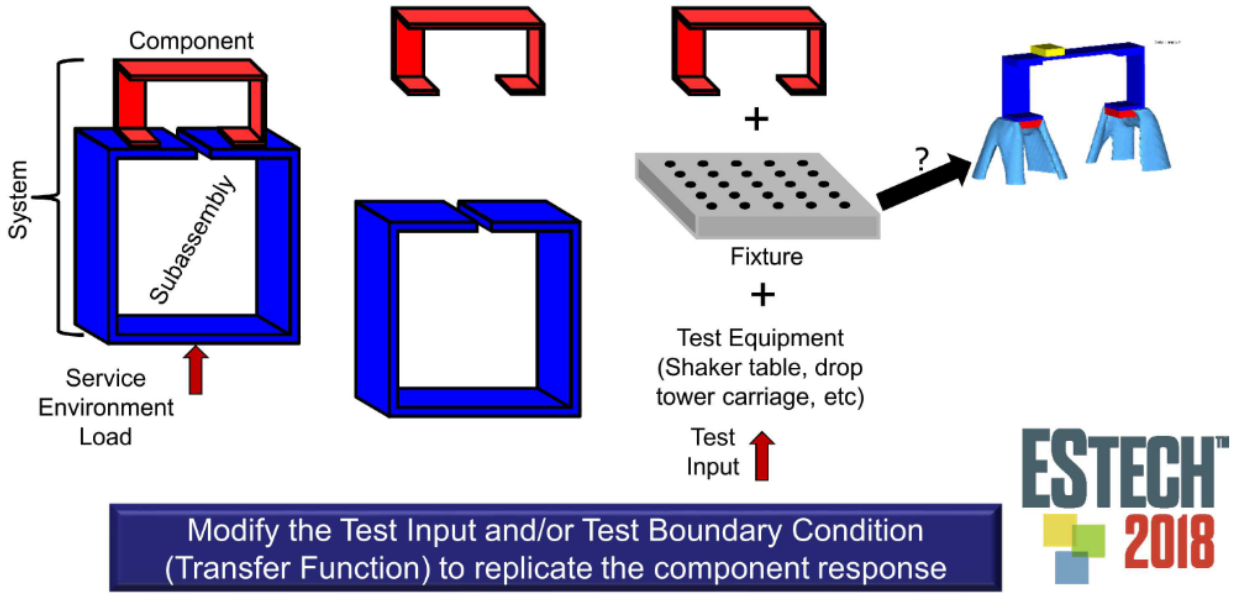

Figure 4: The BARC provides hardware for experimenting with test input and/or boundary condition modification to replicate component response from field environment to laboratory environment (Jones et al., 2018).

The variety of approaches and the lack of a clear best approach saw the need for a common testing apparatus to compare strategies. In 2016, researchers from Sandia National Laboratories and Kansas City National Security Campus developed the boundary condition round-robin challenge problem. They formulated a demonstration

structure that was easy to build and test (Jones et al., 2018). In 2017 a hardware design was finalized: the Box Assembly with Removable Component (BARC) (Soine et al., 2018). The challenge problem, visualized in Figure 4, tasked researchers with modifying the test input and/or boundary condition to replicate the BARC component's measured response between field and lab environments. In the years since its introduction, a large body of literature has been produced for this structure (Rohe et al., 2018).

This thesis's proposed method is an impedance modification approach and builds upon a recent study that utilized one single-axis shaker table and one test, called the Angle Optimization method (Knight et al., 2018). This study proposed a method to test a component at an offset angle. They devised an optimization scheme to select an offset angle which also determined whether the testing sequence required one, two, or all three tests (traditional sequential single-axis testing uses three tests). They found that "the optimum testing configuration resulted in an overall averaged error significantly smaller than the traditional methods. Crucially, this case study shows that the optimum test campaign could be a single equipment level test opposed to the traditional three orthogonal direction tests." This is a promising result and indicates that further test fixture optimization beyond only the offset angle may yield even greater improvements.

While the angle optimization seems a crucial first step, there are a variety of structural optimization techniques that may be used to better design a single-axis test fixture that approximate the multi-axis response experienced in the field environment (Topping, 1992). Topology optimization is one such form of structural optimization (Bendsøe et al., 1999), and recent methods have been applied to optimizing structures subject to dynamic loading due to random vibration (Yang et al., 2017; Gomez et al.,

2019). Topology optimization is a superset of size optimization (which modifies dimensions) and shape optimization (which modifies boundaries), while allowing for the addition or removal of holes. Similarly, layout optimization, which optimizes the placement of geometric objects, has been applied to structures subject to dynamic loads from random vibration (Qiao et al., 2012). Topology optimization for vibration test fixture design has run into problems with computational time and convergence to local minima (Schoenherr, 2020), but a variety of new topology optimization reparameterizations using neural networks have alleviated some of these concerns (Hoyer et al., 2019; Rawat et al., 2019; Chandrasekhar et al., 2020; Nie et al., 2020).

Since a single-axis shaker table will produce response in all three primary axes, and the test fixture boundary condition impacts cross-axis responses, then there likely exists some non-rigid boundary condition that can produce an improved approximation of the service environment when excited by a single-axis shaker.

The angle optimization study showed that a single-axis vibration test of a satellite system was able to adequately match the maximum RMS values for the coupled system tests with only one test at an optimized offset angle (Knight et al., 2018). This thesis's proposed method builds upon the optimized offset angle approach by also dynamically optimizing the test fixture stiffness. The goal is to produce a test which approximates the service environment using one excitation from a single-axis shaker. Figure 5 previews the proposed method via a simple illustration. In the figure, a single shaker input is applied vertically at the base in order to excite a response in the rotated system. Test fixture stiffnesses are optimized to shape responses to better match targets. The

flowchart in Figure 6 breaks down the strategies involved in this method and the motivations for trying them.

The method is called “rapid, approximate multi-axis vibration testing,” although throughout the thesis it is referred to as Single-Input, Multiple-Output (SIMO) multi-axis testing. It is rapid because it requires only one test, saving the time needed to setup and test an article three times. In comparison to a Multiple-Input, Multiple-Output (MIMO) testing method such as IMMAT, the proposed method saves the time required for a more complex setup and execution process. The method is approximate because it is unlikely to result in a test equivalent to one achieved using a multi-axis shaker. The goal of this thesis is to assess the quality of the approximation.

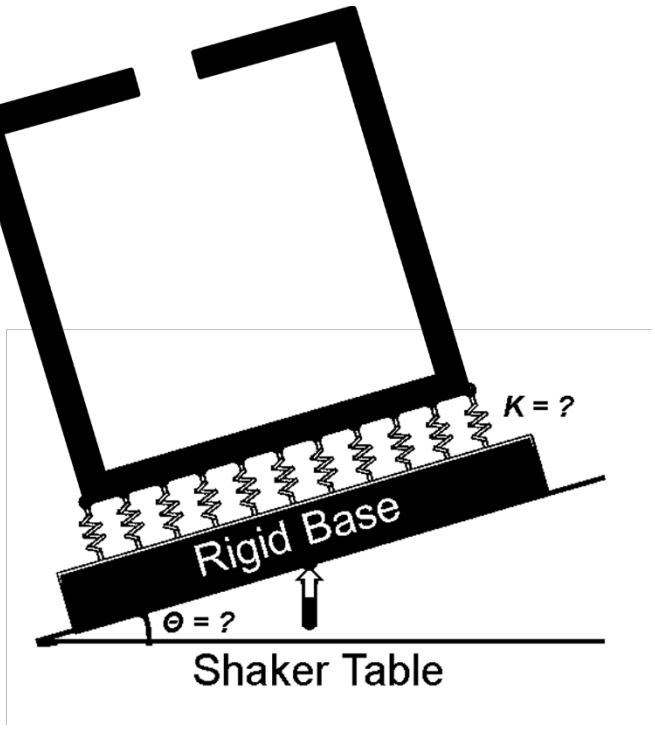

Figure 5: The model is rotated to adjust the relative excitation energy applied to each of the test article’s primary axes.

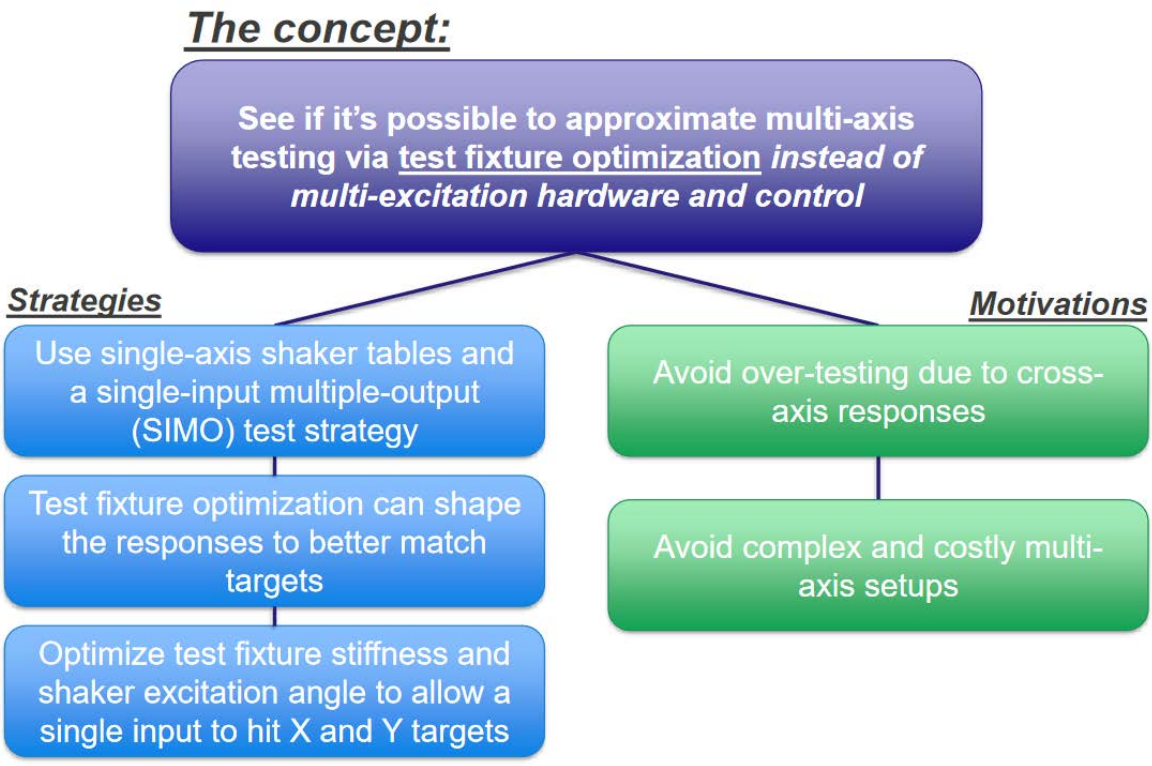

Figure 6: Concept flowchart with strategies and motivations.

Objectives

The objectives of the research are as follows:

- To assess the quality of the proposed method.
- To understand how much test quality improvement is possible with a well-designed test fixture.
- To determine the effect of increasing the number of test fixture optimization parameters.

In order to meet the above objectives, this thesis presents four case studies. The case studies provide insight into (1) the effect of a dynamically optimized test fixture and (2) the effectiveness of an offset angle in the proposed method.

METHOD

Case Studies

Four case studies are presented in order to compare the proposed method to traditional testing approaches, namely, sequential single-axis testing.

Table 1 summarizes the four case studies. Each case study compares sequential single-axis testing to the proposed method, which uses a Single-Input, Multiple-Output (SIMO) multi-axis testing strategy. In the first case study, both tests use a rigid test fixture. Variations in control location are discussed later in the Finite Element Model subsection. In cases 2, 3, and 4 the test fixture undergoes structural optimization with increasing complexity. The goal of these case studies is to (1) assess the quality of the proposed method, (2) to understand how much improvement is possible with a well-designed test fixture, and (3) to determine the effect of increasing the number of optimization parameters.

Table 1: Four case studies.

Case	Test Fixture	Comparison
1	Rigid	Sequential single-axis (single control location) Sequential single-axis (all control locations) SIMO multi-axis (all control locations)
2	Two Stiffness Parameters	Sequential single-axis SIMO multi-axis
3	Four Stiffness Parameters	Sequential single-axis SIMO multi-axis
4	Eight Stiffness Parameters	Sequential single-axis SIMO multi-axis

First, the finite element model must be defined. The Finite Element Model subsection describes the model used in each of the case studies, including mesh properties, dimensions, mode shapes, and measurement locations. The Service Environment subsection discusses how we defined a service environment. The

Boundary Conditions subsection describes which boundary conditions were used, and the parameterization of those boundary conditions for the optimization. Test quality metrics are introduced in the Test Quality Metrics subsection and are used to assess the model's ability to match the defined service environment. Lastly, the Simulation Approach subsection discusses the method for simulating a dynamic environments test on a finite element model.

Finite Element Model

Each case study is performed on a finite element model created using the Abaqus software. The article under test in our model is a 2-dimensional BARC structure, which is a solid aluminum square part with a channel (Rohe, 2018). This test article was chosen due to an abundance of longitudinal and vertical mode shapes within the test's frequency bandwidth. The BARC is also a common test article in dynamic environments testing literature, so there are many related studies to compare to.

The entire finite element model is a 2D assembly consisting of the BARC, a test fixture, and a rigid base. The BARC is meshed with 681 plane strain elements. Table 2 summarizes the finite element properties. Figure 7 shows the first four mode shapes of the model.

Table 2: Finite element properties.

Property	Value
Approximate Cell Size	0.003 m
Number of Elements	681
Element Type	4-node bilinear plane strain quadrilateral, reduced integration, hourglass control (CPE4R in Abaqus)
Material	Aluminum 6061
Outer Dimensions	15.24 x 12.7 cm (Rohe, 2018)

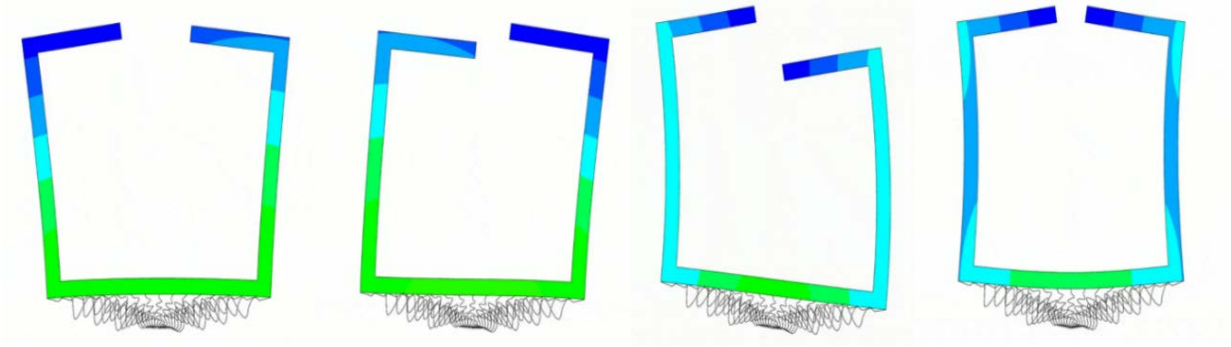

Figure 7: First four mode shapes of the BARC model with their natural frequencies. The X and Y springs all have a stiffness of $\mathbf{k = 10^8\ N/m}$.

A mesh convergence study was performed to determine the optimal mesh density. A finer mesh provides a more accurate modal solution but significantly increases computation time. Four mesh densities were evaluated, and their resulting percent variation from a baseline mesh density are summarized in Table 3. A mesh with an approximate cell size of 0.003 meters, which corresponds to 3 cells through the thickness of the part, resulted in natural frequencies less than 0.5% different from the baseline mesh density, and was therefore considered sufficiently dense as to not influence the validity of the simulation.

Table 3: Mesh convergence study.

Approximate Global Size (m)	# of Cells through Thickness	First Four Natural Frequencies (Hz)				Maximum % Difference from Baseline
0.0025	4	208.68	209.16	974.65	977.16	NA (baseline)
0.003	3	208.69	209.33	972.63	974.09	0%
0.005	2	204.05	204.08	954.11	954.33	2%
0.01	1	183.34	183.37	852.08	852.27	13%

The test fixture is idealized by sixteen springs, each with an independent vertical and longitudinal stiffness. The springs are spring-dashpot engineering elements with no

damping. The test fixture is attached to a rigid base, which represents the shaker table. The base is modeled as a 10,000 kg analytical rigid shell and is stiffly connected to the ground. Since the base is meant to represent a vertically-oriented, single-axis shaker table, the acceleration input is always applied vertically at the base.

In a physical test, accelerometers are placed on the test article's surfaces to measure acceleration response due to shaker table input. A response-matching test tries to match a desired target response at some set of control locations. Control accelerometers are used to control the measured response a shaker should try to produce at the test article's control locations. Therefore, measurement locations and control locations differ in that the simulation attempts to drive a target response at the control locations, while the measurement locations simply measure response.

In our model, accelerometers are represented as nodes, and acceleration transfer functions are computed between the rigid base and the selected measurement location nodes. These transfer functions are used to compute the response at any given measurement location due to a known input at the base. Thirty-four measurement locations were chosen: seventeen evenly spaced along the outside edge and seventeen evenly spaced on the inside edge as shown by the red points on Figure 8. The rigid base has one measurement location at the center which is used as a reference location to compute transfer functions between the BARC and the base. Initially, transfer functions are computed using the modal solution provided by the Lanczos eigensolver, then acceleration responses are calculated at each measurement location by passing the shaker table input, which is a power spectral density (PSD), through those transfer functions.

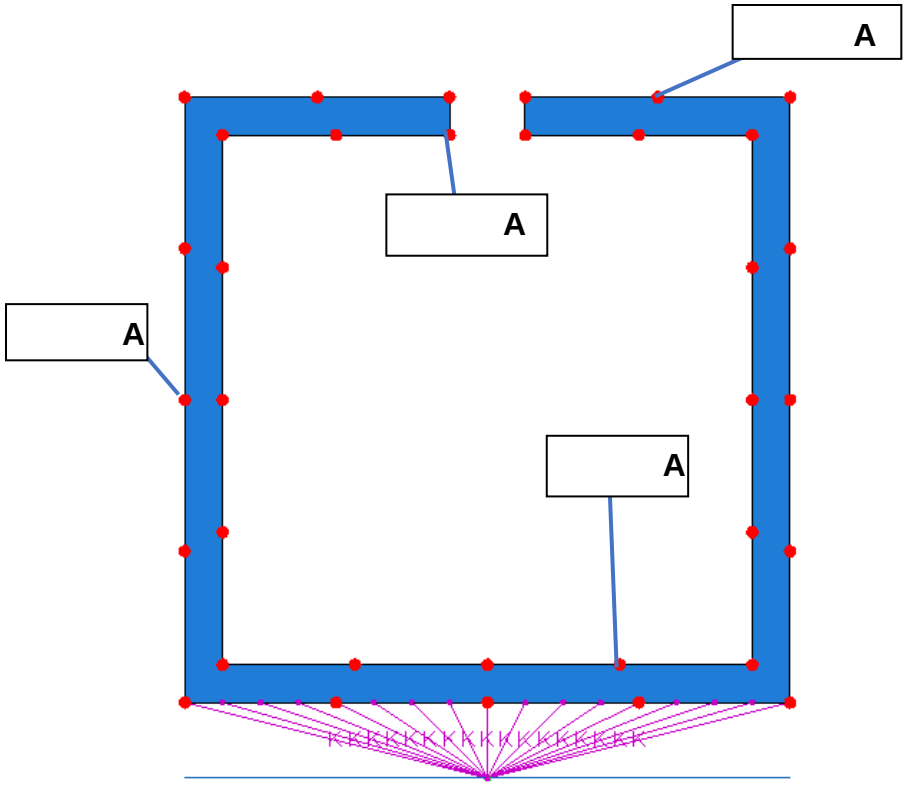

Figure 8: BARC model with measurement locations shown in red. Four specific locations are called out.

In a typical physical test, only a single control location is chosen. This means the test does a very good job of achieving a target response at one location, but neglects responses at other locations on the body. Test engineers usually use a single control location for two reasons. One is that testing software is often unable to control to more than one location. The second reason is that test specifications often fail to provide targets at multiple locations, which may be due to a lack of instrumentation at multiple locations in field tests. Typically, control locations are chosen to be accessible and instrumentable in both the service and laboratory settings. For the first case study, the rigid test fixture case, we subset the results into two categories: (1) single control location and (2) all control locations. In the single control location case, we mimic common test practice, which is to use one control location. The shaker input is derived

to achieve the lowest possible error between the target and response at the chosen location. Importantly, this derivation is dependent on the test quality metric used. This thesis derives all inputs to minimize RMS dB error, which is discussed more in the Test Quality Metrics subsection. In the all control locations case we allow the simulation to control the response at all thirty-four nodes. The shaker input is derived to achieve the lowest possible error between the target and response averaged at all locations. Controlling at all locations necessarily results in a better overall test, assuming the goal is to minimize error across the whole body and not just at a single location.

For the single control location test, there is a large difference between the “best performing” control location and the “worst performing.” This is something not often considered when instrumentation locations are selected for a field test, because, as previously mentioned, locations are selected to be accessible and instrumentable, not because they will result in a good test across the body. The location selected for test control has a large impact on test quality. In the Results section, we compare single and all control locations, as well as best and worst performing single location.

Service Environment

A service environment is a real environment the test article is expected to experience in its lifetime. In each case study, the target is a representative service environment. We chose a target with a few orders of magnitude of variation between the target responses at each measurement location in both the longitudinal (X) and vertical (Y) directions. This varied target provides a realistic yet challenging set of responses to achieve. The targets are generated using the MIL-STD-810H Common Carrier environment shown in Figure 9 (Defense Logistics Agency, 2019).

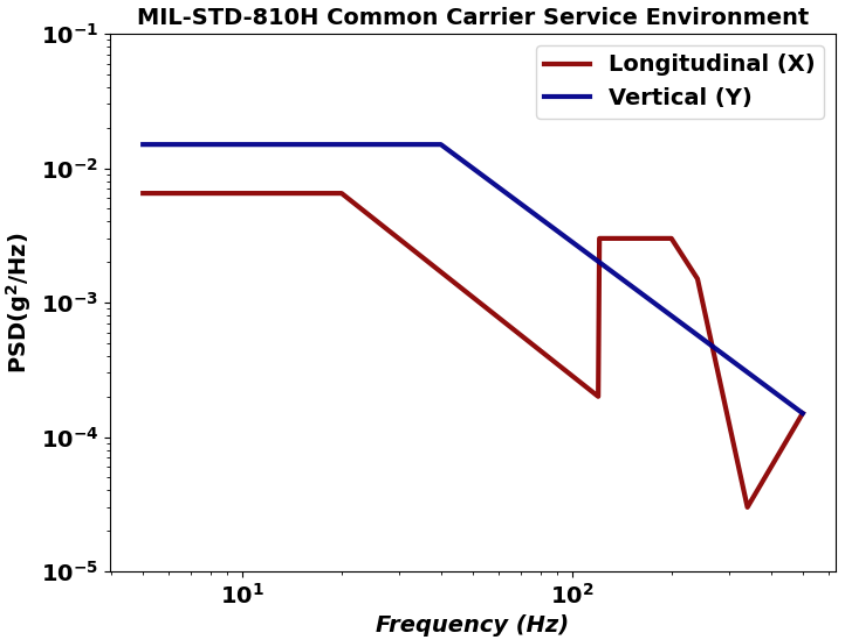

Figure 9: Common carrier (US Highway Truck) service environment (Defense Logistics Agency, 2019).

This is a commonly used service environment to qualify test articles for transportation in the bed of a truck. In order to define a response-matching test for this service environment's base excitation, the longitudinal and vertical PSD of this service environment were transformed into time series acceleration data and simultaneously applied as an input at the base. Acceleration time responses at each measurement location were recorded then transformed back into PSDs with a frequency bandwidth from 10 Hz to 500 Hz. The resulting set of PSDs are shown in Figure 10. The goal of this target generation approach was to produce a set of test article responses in a representative multi-axis service environment to be recreated in a response-matching laboratory test.

This set of targets was generated using a flexible boundary condition. All test fixture springs had an X- and Y-stiffness of $10^6\ N/m$, which was chosen to achieve a boundary condition halfway between a fixed-fixed and free-free condition. This type of

flexible boundary condition is common in real systems and often leads to responses that are difficult to match in a laboratory test.

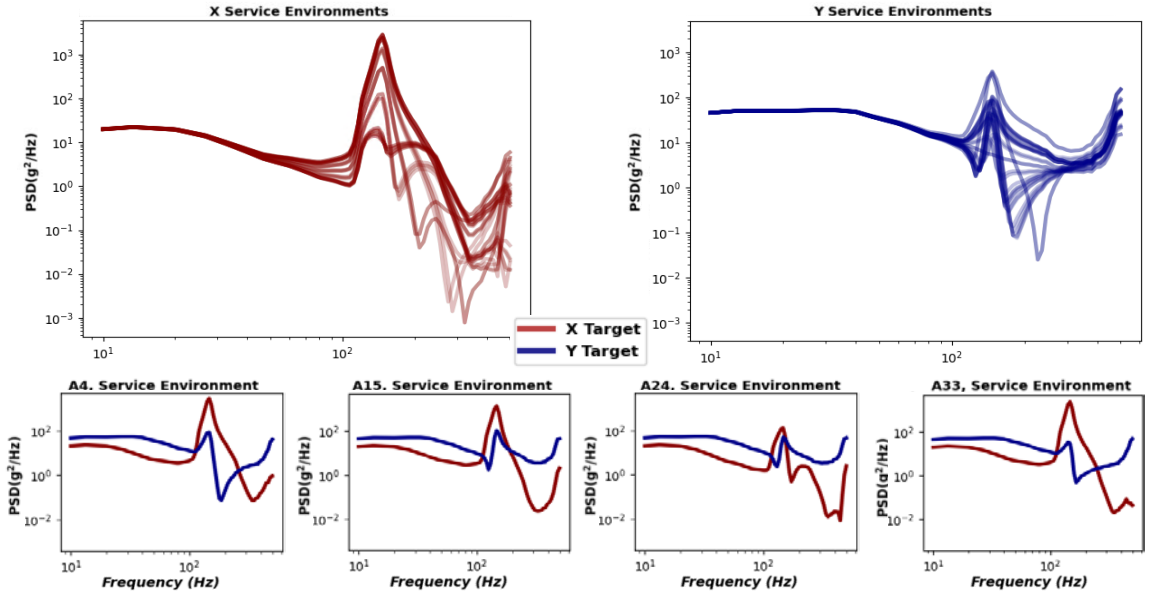

Figure 10: Service environments derived from simultaneous X and Y input of the MIL-STD-810H common carrier service environment at the base of the finite element model. The bottom row shows X and Y targets at the locations called out on Figure 8.

Boundary Conditions

In a laboratory test, the test article's boundary conditions are determined by the test fixture. Test fixtures are typically rigid even though the real boundary conditions experienced in the service environment are often flexible. In our model, the boundary condition is determined by the stiffness of the test fixture springs. We selected a range of boundary condition stiffnesses between free-free and fixed-fixed, and in cases 2, 3, and 4 a brute force search is used to find the combination of stiffness values which produces the lowest RMS dB error. In the first case study, all springs are in their fixed-fixed (rigid) condition. In the second case study the simulation searches for an optimal vertical stiffness (k_y) and longitudinal stiffness (k_x). In the third case study, both the

longitudinal and vertical groups are split in half, providing four optimization parameters ($k_{x1}, k_{x2}, k_{y1}, k_{y2}$). In the fourth and final case study, the groups are split again, providing eight optimization parameters ($k_{x1}, k_{x2}, k_{x3}, k_{x4}, k_{y1}, k_{y2}, k_{y3}, k_{y4}$). Figures 11 and 12 show the assigned groupings of test fixture stiffnesses. Table 4 summarizes the boundary condition and optimization parameters of each case study.

The goal of this boundary condition variation is to determine how much test fixture complexity contributes to improving the possible solutions, although it is also important to consider that an increased number of optimization parameters exponentially increases the computational time needed to search the solution space.

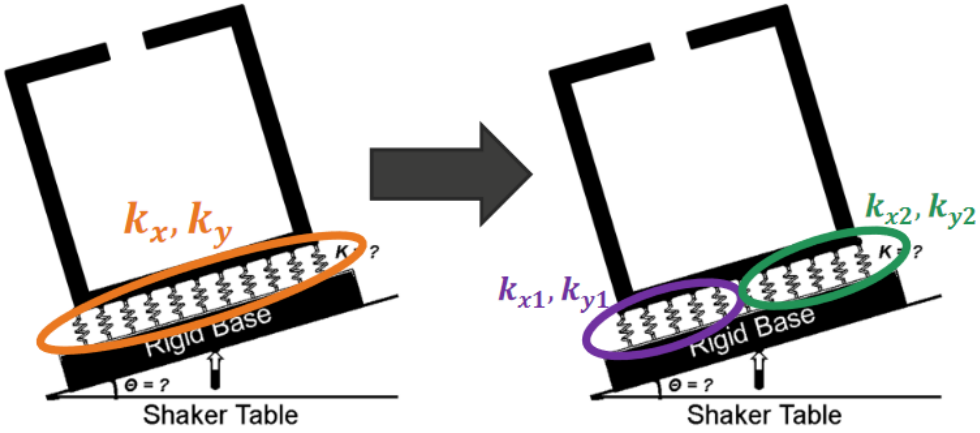

Figure 11: Increase from two stiffness parameters to four stiffness parameters.

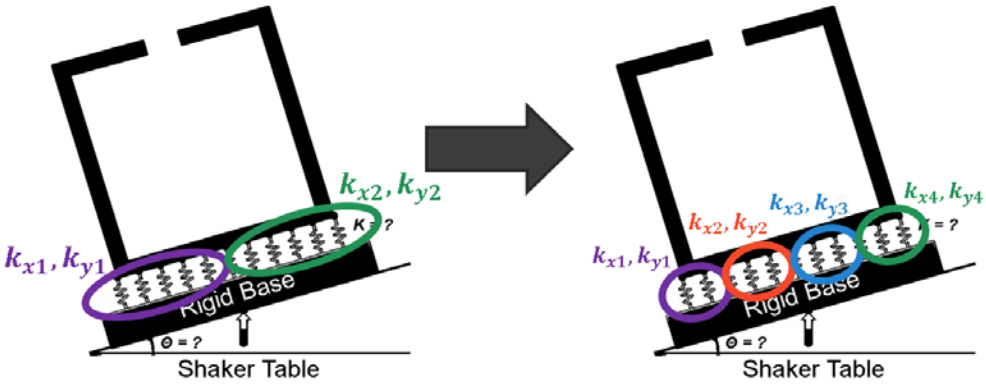

Figure 12: Increase from four stiffness parameters to eight stiffness parameters.

Table 4: Boundary conditions and optimization parameters for each case study.

Case	Test Fixture	Optimization Parameters	
		Sequential Single-Axis	SIMO Multi-Axis
1	Rigid		θ
2	Two Stiffness Parameters	k_x, k_y	k_x, k_y, θ
3	Four Stiffness Parameters	$k_{x1}, k_{x2}, k_{y1}, k_{y2}$	$k_{x1}, k_{x2}, k_{y1}, k_{y2}, \theta$
4	Eight Stiffness Parameters	$k_{x1}, k_{x2}, k_{x3}, k_{x4}, k_{y1}, k_{y2}, k_{y3}, k_{y4}$	$k_{x1}, k_{x2}, k_{x3}, k_{x4}, k_{y1}, k_{y2}, k_{y3}, k_{y4}, \theta$

To adjust the relative amount of excitation energy applied to the X-axis and Y-axis, the model is rotated such that the vertical shaker excitation is applied to the entire system at an angle. The angle of this rotation is optimized using a brute force search over every angle between 0 and 90 degrees in 1 degree increments. In general, the stiffness and angle optimizations can be treated independently, since only the stiffness optimization affects the mode shapes of the system. The angle optimization adjusts the relative amount of excitation energy applied in each direction. When stiffness and angle are optimized together, the stiffness optimization occurs in an outer loop and the angle optimization in an inner loop. For every combination of stiffness values, the optimization checks every angle for a best solution before trying the next stiffness combination.

Test Quality Metrics

Two scalar measures of test quality are introduced to quantify the difference between test targets and responses: RMS dB Error (RDBE) and the percentage of frequency lines within a 3 dB tolerance (% FL).

The RMS dB Error between two PSDs can be calculated to supply a scalar metric sensitive to large differences on a log scale. The RMS dB error value between a

response PSD and a target PSD is a representation of the average mismatch between the response and the target across all frequencies.

In equation 1, $\hat{y}_i$ is the value of a response PSD at the i^{th} frequency line, and y_i is the value of the target PSD at the i^{th} frequency line. The squared decibel error between the response and target PSDs is summed at every frequency line up to the n^{th} frequency line. The resulting sum is divided by the total number of frequency lines, n, and the square root of that quantity is the RMS dB error.

$$RDBE = \sqrt{\frac{\sum_{i=1}^{n} (10 \log_{10} \frac{\hat{y}_i}{y_i})^2}{n}} \quad (1)$$

Another metric employed is the percentage of frequency lines within a 3 dB tolerance. This metric counts the percentage of frequency lines where the response PSD differs from the target PSD by less than 3 dB. While the RDBE metric should be minimized to improve test quality, % FL should be maximized.

$$\%\, FL = \; 100 * \frac{1}{n} \sum_{i=1}^{n} \begin{cases} 1 \; if \; \left| 10 \log_{10} \frac{\hat{y}_i}{y_i} \right| \leq 3 \; dB \\ 0 \; if \; \left| 10 \log_{10} \frac{\hat{y}_i}{y_i} \right| > 3 \; dB \end{cases} \quad (2)$$

In each test simulation, the input PSD is derived to minimize RDBE across control locations, which is not necessarily optimal for maximizing % FL.

Simulation Approach

The primary goal of this paper is to compare sequential single-axis testing to the proposed method. In the sequential single-axis test, the axes are tested one at a time, and two shaker table inputs are derived—one to hit the X-axis target and one to hit the Y-axis target. In the SIMO multi-axis test, a single input is derived to hit both targets

simultaneously. To adjust the relative amount of excitation energy applied in both directions, the model is rotated such that the vertical shaker excitation is applied to the entire system at an angle. This method is visualized in Figure 13 where $\theta = 0°$ correspond to excitation in the BARC's local Y-axis, and $\theta = 90°$ correspond to excitation in the BARC's local X-axis.

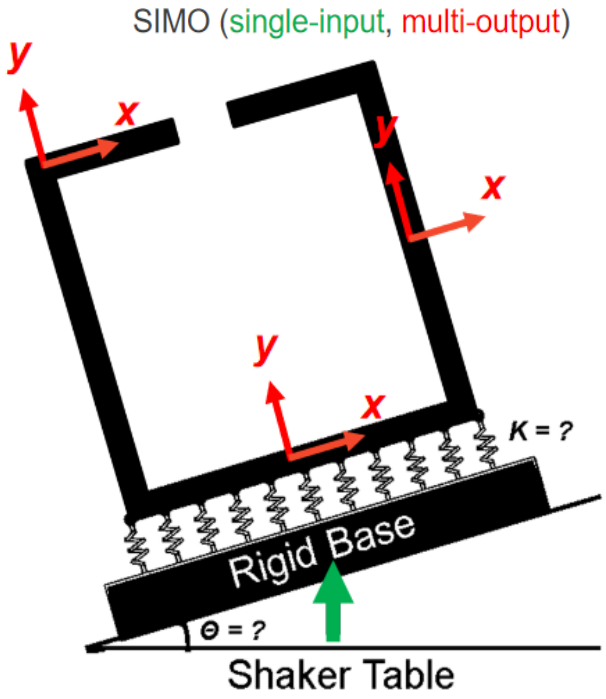

Figure 13: The single shaker table input is shown in green and the multiple outputs are shown in red. The goal of the method is to achieve a set of target responses across multiple control points in multiple directions.

In both cases, the input is derived by passing the target responses through the inverse acceleration transfer functions at each control location. The resulting acceleration PSDs are the shaker table inputs needed to produce the target response at each control location. A log-mean of this set of inputs is computed over the control locations to produce one shaker table input.

RESULTS

Case 1 Results

Table 5 compares the results of a sequential single-axis test with a rigid test fixture when using various single control locations. The rigid test fixture has stiffness values, $k_x = k_y = 10^9\ N/m$. The control location that resulted in the best and worst mean RMS dB error are compared. The X-Error column contains the test quality metrics averaged across all X-axis degrees of freedom, and the Y-Error column contains the test quality metrics averaged across all Y-axis degrees of freedom. The Mean Error column is the average of the X- and Y-axis errors. The mean RMS dB error improved by 2.2 dB from the worst control location to the best.

Table 5: Comparison of best and worst control locations for the sequential single-axis test with a rigid test fixture.

Sequential Single-Axis (Worst performing control location)				Sequential Single-Axis (Best performing control location)			
	X-Error (avg)	Y-Error (avg)	Mean Error		X-Error (avg)	Y-Error (avg)	Mean Error
RDBE	9.9 dB	3.2 dB	6.6 dB	RDBE	5.6 dB	3.2 dB	4.4 dB
FTOL	64.6%	83.9%	74.3%	FTOL	71.6%	84.7%	78.2%

In Case 1, even further improvement is gained by controlling to all locations instead of choosing one. In this case, a baseline test is carried out for both the sequential single-axis test and the SIMO multi-axis test using a rigid test fixture. No structural optimization is performed. Both test fixtures have stiffness values, $k_x = k_y = 10^9\ N/m$. In the SIMO multi-axis case, the angle is still optimized to tune the excitation energy applied to the X- and Y-axis of the BARC. The optimal angle was found to be $\theta = 27°$.

Table 6 summarizes the results of both tests. In Table 6, the sequential test using

all control locations has a lower average RMS dB error than the best-case single control location test from Table 5. The SIMO multi-axis test has an average RMS dB error greater than the sequential case by 1.0 dB. As noted, this error was expected to be higher because it only accounts for the on-axis error of each test. A sequential test using an X and a Y test will always result in lower X and Y error, respectively, than the SIMO multi-axis test using a single test.

Table 6: Case 1 compares a sequential single-axis test to a SIMO multi-axis test when using a rigid test fixture. The test fixture was assigned stiffness values $k_x = 10^9\ N/m$ and $k_y = 10^9\ N/m$.

Case 1 – Rigid Test Fixture							
Sequential Single-Axis				SIMO Multi-Axis			
	X-Error (avg)	Y-Error (avg)	Mean Error		X-Error (avg)	Y-Error (avg)	Mean Error
RDBE	5.1 dB	2.6 dB	3.8 dB	RDBE	5.7 dB	3.9 dB	4.8 dB
FTOL	70.3%	85.2%	77.8%	FTOL	69.2%	78.7%	74.0%

This decrease in measured test quality metrics may be justified because the SIMO multi-axis test eliminates cross-axis responses that are unavoidable in the sequential test. The cross-axis responses have a significant impact on test quality, which we summarized in the introduction, but due to the nature of the test quality metrics, we are unable to quantify them. Both the RMS dB error and frequency lines within tolerance test metrics are computed on a decibel scale, and since the target cross-axis response in a single-axis test is zero, all decibel errors are infinite and the percentage of frequency lines within tolerance is 0%. A future study may want to devise a test quality metric which can account for the off-axes responses.

Case 2 Results

In Case 2, the X and Y stiffness values of the test fixture springs were optimized to minimize RMS dB error for the sequential and SIMO cases. The optimization searched 225 combinations of k_x and k_y. For the sequential single-axis test, the optimization found an optimal test fixture with stiffness values $k_x = 3.2 * 10^4\ N/m$ and $k_y = 2.7 * 10^6\ N/m$. For the SIMO multi-axis test, the optimization found an optimal test fixture with stiffness values $k_x = 1.2 * 10^7\ N/m$, $k_y = 2.7 * 10^6\ N/m$, and $\theta = 27°$.

One instance of the angle optimization surface for the Case 2 SIMO multi-axis test is visualized in Figure 14. The angle objective function is convex and has a clear minimum.

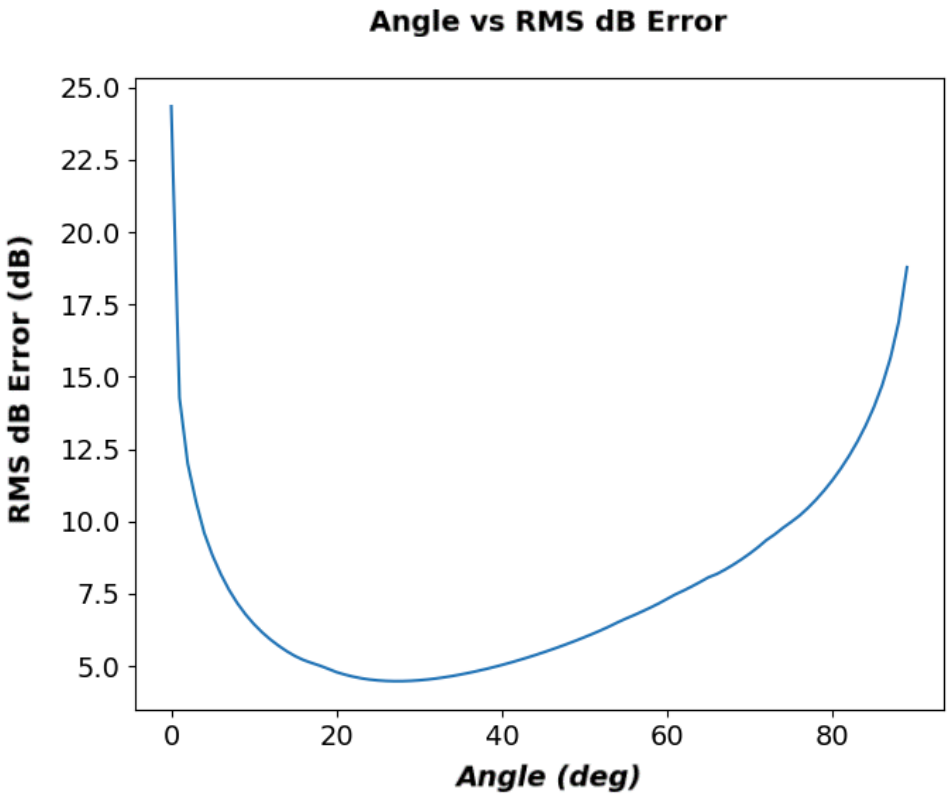

Figure 14: RMS dB error is minimized by adjusting the excitation angle. A clear minimum is found at $\theta = 27°$.

Table 7 summarizes the resulting test quality metric values. An improvement is gained over the rigid test fixture used for Case 1 for both the sequential and SIMO test. For the sequential test, the RMS dB error improves slightly in both axes, and the percentage of frequency lines within a 3 dB tolerance increases by 2.2%. For the SIMO test, the RMS dB error improves by 0.3 dB in the X-axis and 0.4 dB in the Y-axis, and the percentage of frequency lines within a 3 dB tolerance increases by 1.5.

These results indicate that the test fixture optimization was able to improve the SIMO test slightly more than the sequential test, although improvements were made in both tests.

Table 7: RMS dB error (RDBE) and percentage of frequency lines within a 3 dB tolerance (FTOL) for Case 2. Case 2 compares a sequential single-axis test to a SIMO multi-axis test when the test fixture is dynamically optimized using two stiffness parameters.

Case 2 – Two Stiffness Parameters							
Sequential Single-Axis				SIMO Multi-Axis			
	X-Error (avg)	Y-Error (avg)	Mean Error		X-Error (avg)	Y-Error (avg)	Mean Error
RDBE	5.0 *dB*	2.5 *dB*	3.7 *dB*	RDBE	5.4 *dB*	3.5 *dB*	4.5 *dB*
FTOL	74.5%	85.5%	80.0%	FTOL	69.9%	81.4%	75.5%

The grid of stiffness values searched for Case 2 is shown in Figures 15 and 16. In these figures, the Y stiffness values are on the plot's X-axis and the X stiffness values are on the plot's Y-axis. The light green color represents low RMS dB error values, while the red color represents high RMS dB error values.

Figure 15 shows the heat map of error values for the sequential single-axis test. This plot indicates that the X-axis stiffness had little effect on the RDBE metric, while the Y-axis stiffness had a large effect depending on whether or not it was above or below $1.4 * 10^5\ N/m$. There are two large regions of solutions, with low error occurring when

the Y stiffness was above $1.4 * 10^5\ N/m$ and high error occurring when the Y stiffness was below $1.4 * 10^5\ N/m$.

Figure 16 shows the heat map of error values for the SIMO multi-axis test. There is necessarily no stiffness solution where the SIMO test outperforms the sequential test, but there are clear regions of solutions where they are competitive. The SIMO test has a minimum region when $k_y = 2.7 * 10^6\ N/m$ and k_x is close to $1.2 * 10^7\ N/m$.

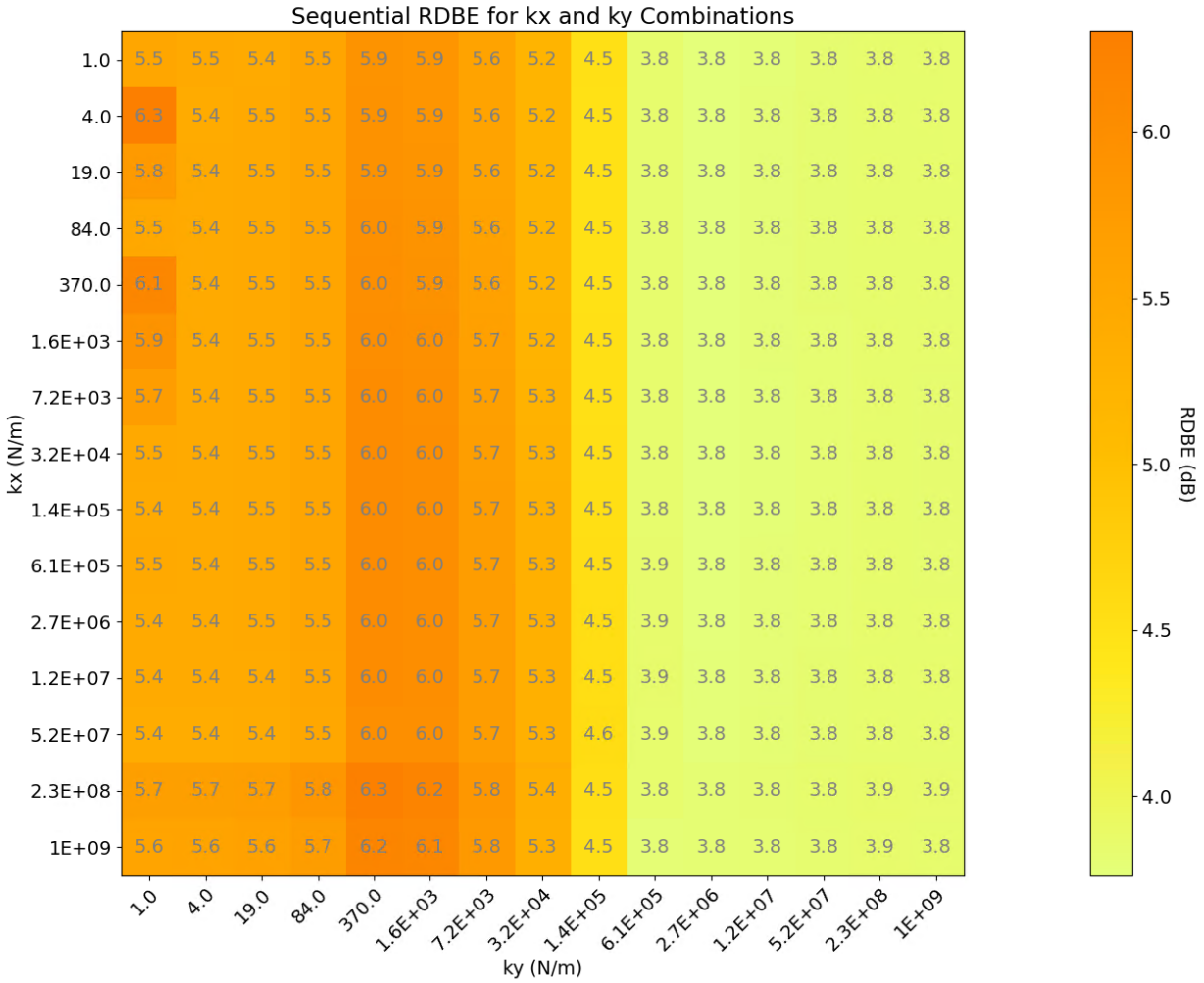

Figure 15: Grid of RMS dB errors for all Case 2 stiffness combinations for the sequential single-axis case.

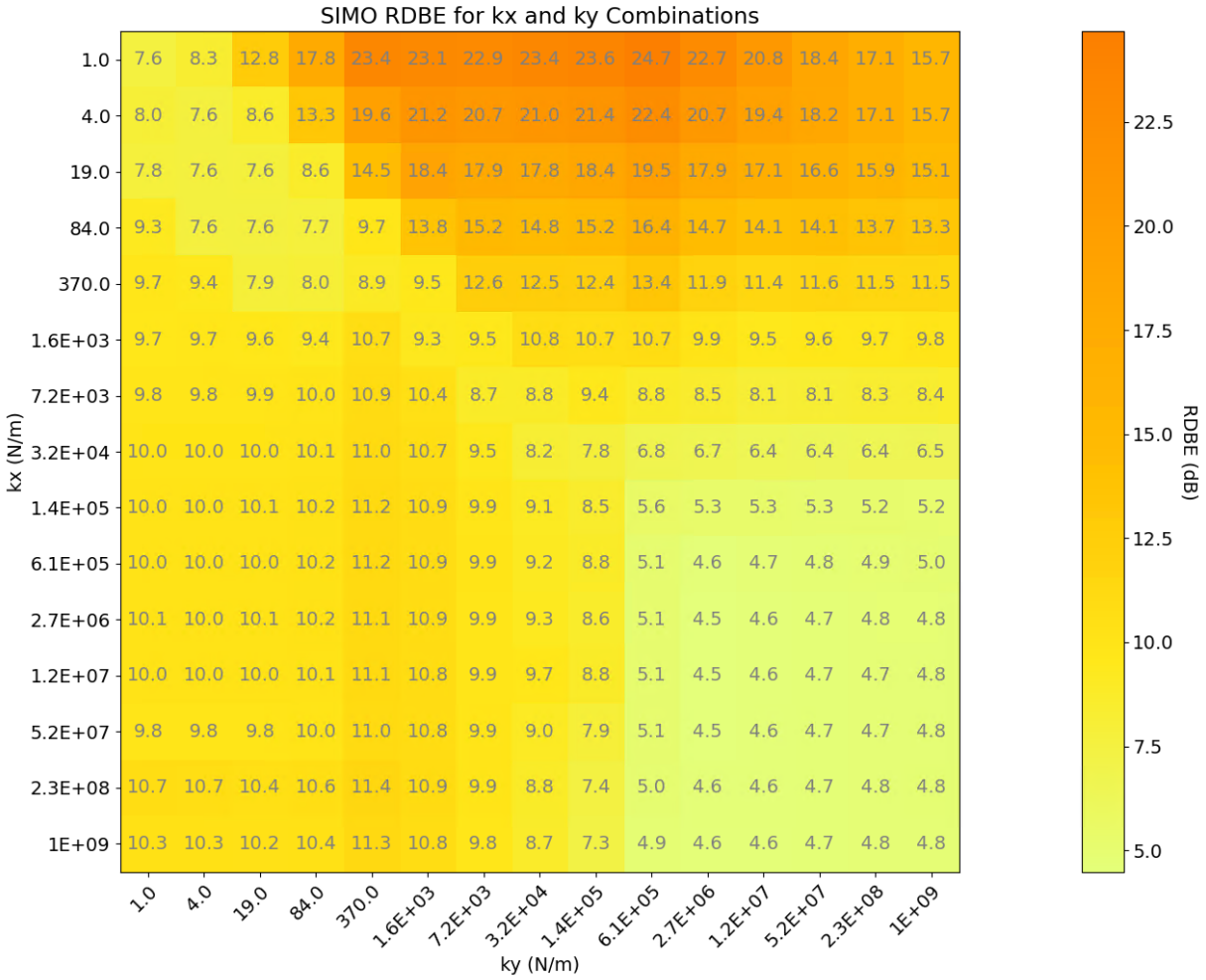

Figure 16: Grid of RMS dB errors for all Case 2 stiffness combinations for the SIMO multi-axis case.

This heat map gives a coarse view of the objective function, which appears fairly smooth over the search range. The soft spring cases produce notably worse errors, which decrease rapidly toward a minimum. The errors start to increase again as the springs approach rigid.

Case 3 Results

In Case 3, the test fixture was further parameterized to allow the optimization finer control over the test fixture's dynamics. The optimization searched over 50,625

combinations of stiffness parameters. With four stiffness parameters, the optimization failed to improve upon the sequential single-axis and the SIMO multi-axis test from Case 2. These results are summarized in Table 8.

The optimal stiffness values for the single-axis test were $k_{x1} = 3.2 * 10^4\ N/m,\ k_{x2} = 1\ N/m,\ k_{y1} = 2.7 * 10^6\ N/m,\ k_{y2} = 2.7 * 10^6\ N/m$.

The SIMO test did not improve over Case 2, with overall RMS dB error staying the same, and the frequency lines within tolerance increasing. This solution was found with stiffness values: $k_{x1} = 19\ N/m,\ k_{x2} = 2.3 * 10^8\ N/m$, $k_{y1} = 2.7 * 10^6\ N/m,\ k_{y2} = 2.7 * 10^6\ N/m$, and $\theta = 27°$.

Table 8: RMS dB error (RDBE) and percentage of frequency lines within a 3 dB tolerance (FTOL) for Case 3. Case 3 compares a sequential single-axis test to a SIMO multi-axis test when the test fixture is dynamically optimized using four stiffness parameters.

Case 3 – Four Stiffness Parameters							
Sequential Single-Axis				SIMO Multi-Axis			
	X-Error (avg)	Y-Error (avg)	Mean Error		X-Error (avg)	Y-Error (avg)	Mean Error
RDBE	5.0 dB	2.5 dB	3.7 dB	RDBE	5.4 dB	3.6 dB	4.5 dB
FTOL	74.5%	85.5%	80.0%	FTOL	69.6%	81.7%	75.6%

Case 4 Results

Case 4 increased the number of optimization parameters to eight. The optimization searched 390,625 combinations of stiffness parameters. The results are summarized in Table 9.

Once again, the optimization failed to improve the best RMS dB error from cases 2 and 3 for the sequential test: 3.7 dB, although this error was achieved with a different solution than the one found in cases 2 and 3. This solution was found with stiffness

values: $k_{x1} = 1\ N/m,\ k_{x2} = 1\ N/m,\ k_{x3} = 1\ N/m,\ k_{x4} = 1\ N/m$, and $k_{y1} = 1\ N/m,\ k_{y2} = 10^9\ N/m,\ k_{y3} = 10^9 N/m,\ k_{y4} = 1\ N/m$.

For the SIMO test, the optimization made no improvements to both the percentage of frequency lines within tolerance and the RMS dB error. This indicates that further increasing the number of stiffness parameters may lead to diminishing returns. This solution was found with stiffness values: $k_{x1} = 10^9\ N/m,\ k_{x2} = 3.2 * 10^4\ N/m,\ k_{x3} = 2.7 * 10^6\ N/m,\ k_{x4} = 2.7 * 10^6\ N/m$, $k_{y1} = 2.7 * 10^6\ N/m,\ k_{y2} = 2.7 * 10^6\ N/m,\ k_{y3} = 10^9\ N/m,\ k_{y4} = 2.7 * 10^6 N/m$, and $\theta = 27°$.

Table 9: RMS dB error (RDBE) and percentage of frequency lines within a 3 dB tolerance (FTOL) for Case 4. Case 4 compares a sequential single-axis test to a SIMO multi-axis test when the test fixture is dynamically optimized using eight stiffness parameters.

Case 4 – Eight Stiffness Parameters							
Sequential Single-Axis				SIMO Multi-Axis			
	X-Error (avg)	Y-Error (avg)	Mean Error		X-Error (avg)	Y-Error (avg)	Mean Error
RDBE	4.9 dB	2.6 dB	3.7 dB	RDBE	5.4 dB	3.6 dB	4.5 dB
FTOL	74.4%	85.0%	79.7%	FTOL	69.5%	81.1%	75.3%

DISCUSSION

Four case studies were presented to compare sequential single-axis testing to the proposed method, Single-Input, Multiple-Output (SIMO) multi-axis testing. In each Case Study, a 2D finite-element BARC test article was used to simulate a dynamic environments test on a single-axis shaker table. In the sequential tests, a shaker input excited the test article in the X-axis and Y-axis sequentially. In the SIMO multi-axis tests, a vertical shaker input excited the test article at an offset angle such that a single input produced response in the X-axis and Y-axis simultaneously. A simultaneous test of multiple axes is desirable because it eliminates the excess lifetime damage from cross-axis responses over several sequential tests.

The key findings are visualized on Figure 17 and 18. The first two case studies show the average RDBE and average FTOL improving when test fixture optimization is performed, but not improving with additional stiffness parameters. This indicates that the optimization is not improved by greater control over the test fixture complexity. Either the solution space is adequately represented by the two stiffness parameter case, or else the true contours of the space are invisible in this coarse of a search.

It's crucial to reiterate that only the on-axis errors are considered here. The off-axes responses for the sequential case are significant and cause over-testing, but because there is not a non-zero off-axis target for sequential tests, they are not quantifiable with the test quality metrics presented.

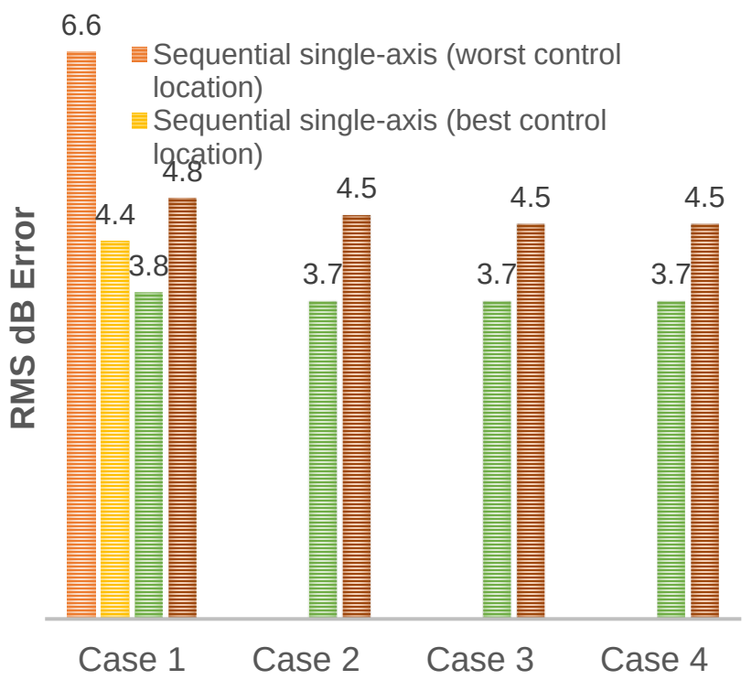

Figure 17: Average RMS dB Error for each case study.

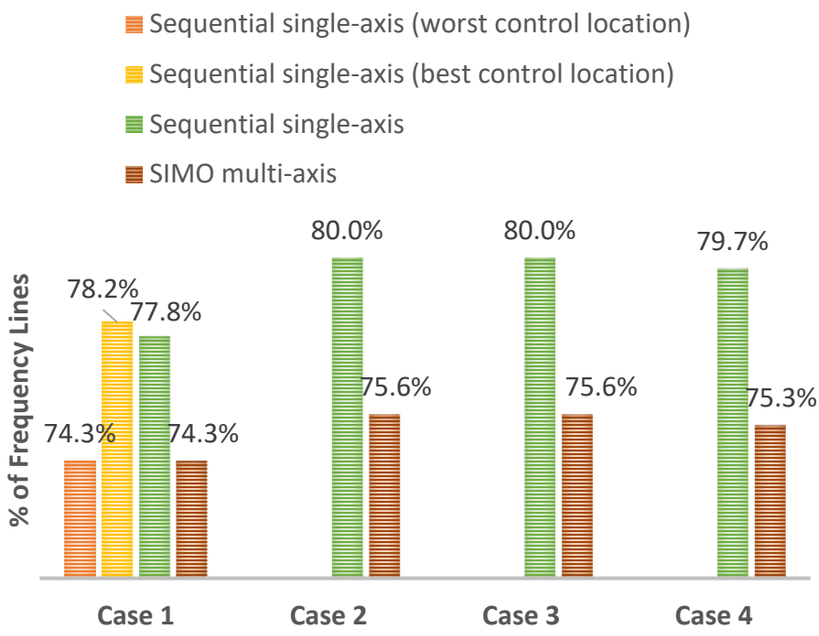

Figure 18: Average percentage of frequency lines within a 3 dB tolerance for each case study.

The primary motivation for this thesis was to investigate the possibility of replacing a series of sequential single-axis tests with a SIMO multi-axis test. When looking only at on-axis responses for a SIMO multi-axis test, the test will always appear worse than the same test performed sequentially. However, when cross-axis responses are considered, as in Figures 19, 20, and 21, it becomes difficult to dismiss the benefit of the SIMO multi-axis test. Compare the responses of the Case 1 sequential single-axis tests in Figure 19 and 20 to the Case 2 SIMO multi-axis test in Figure 21. Although the on-axis responses in the sequential tests closely match the service environment, the cross-axis responses are large. In the SIMO test, the responses approximate the service environment, but since only one test was performed, there are no cross-axis responses.

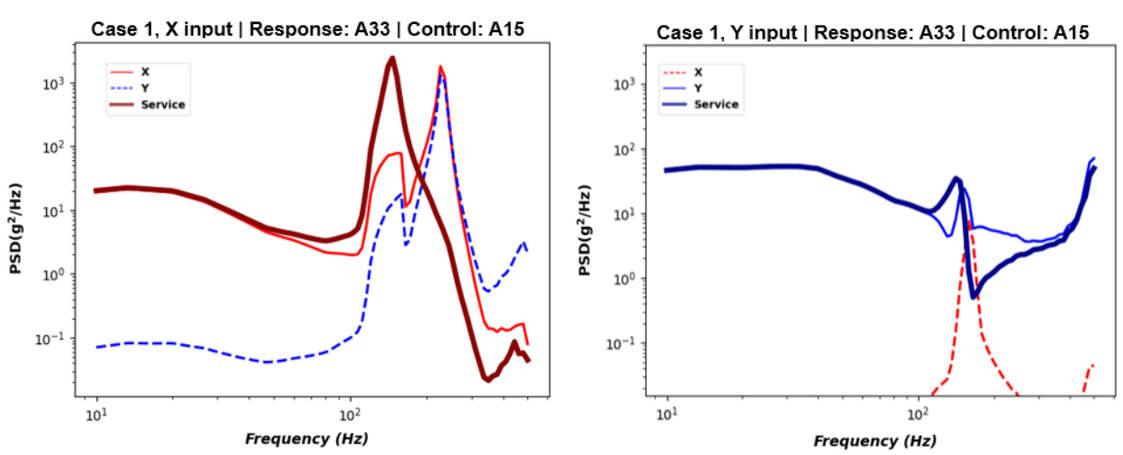

Figure 19: A33 response during Case 1 sequential single-axis, controlled at A15. The off-axis response is dashed. In both tests, at frequencies above 100 Hz, the off-axis responses occasionally exceed the on-axis target.

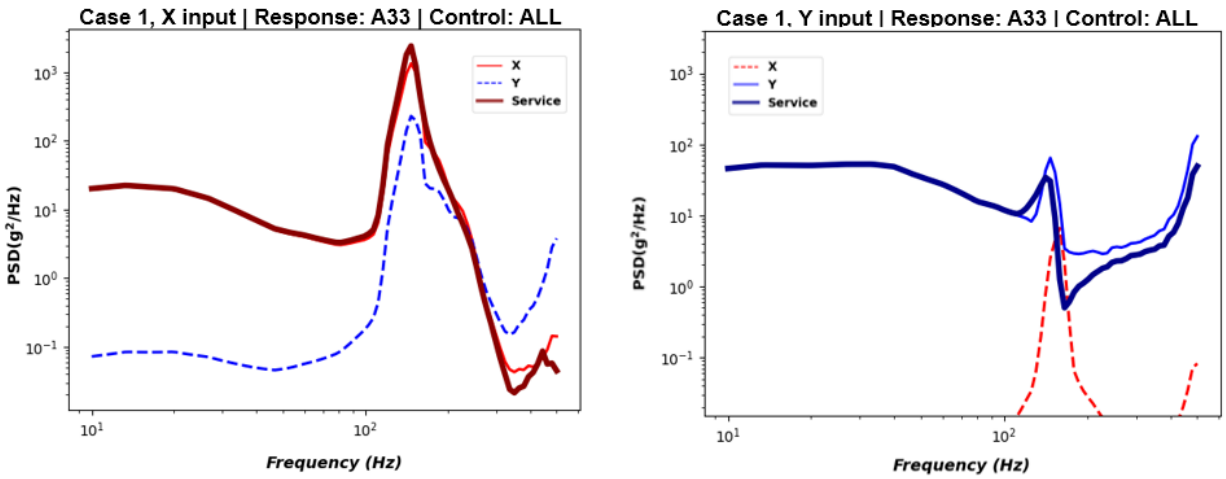

Figure 20: A33 response during Case 1 sequential single-axis, controlled at all locations. The off-axis response is dashed. In both tests, at frequencies above 100 Hz, the off-axis responses occasionally exceed the on-axis target.

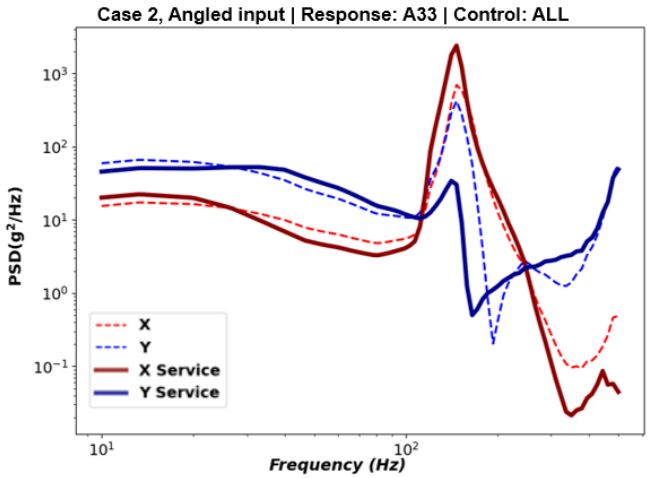

Figure 21: A33 response during Case 2 SIMO multi-axis, controlled at all locations. The dashed lines are the X and Y responses to a single, angled input.

The combined message of the response plots in Figures 19, 20, and 21 and the key test quality metrics in Figures 17 and 18 is that significant over-testing can be avoided for a small on-axis error penalty. In these simulations, the on-axis error penalty for a SIMO multi-axis test was never greater than 1.0 dB and fell to 0.8 dB when test fixture optimization was performed. If one considers that current industry practice for aerospace vibration tests is to use one control location, and often not the best control

location, then the SIMO multi-axis case was on par with or even better than our simulation of an industry test. This research shows that a SIMO multi-axis approximation is feasible with a small error penalty, but stiffness optimization and angle optimization are critical aspects of the method.

Choosing a poor test fixture stiffness or excitation angle can result in a massive increase in error. For the SIMO test, it is critical that both of these design components are considered. Figure 22 shows the SIMO responses when choosing a poor stiffness condition while still optimizing the angle. Similarly, Figure 23 shows the SIMO responses when choosing a poor angle while still optimizing the stiffness. In both cases, the X-response is far below the X-axis service environment, while the Y-response is far above the Y-axis service environment. The stiffness and angle optimization work in tandem to tune the proportion of energy between the X and Y response directions.

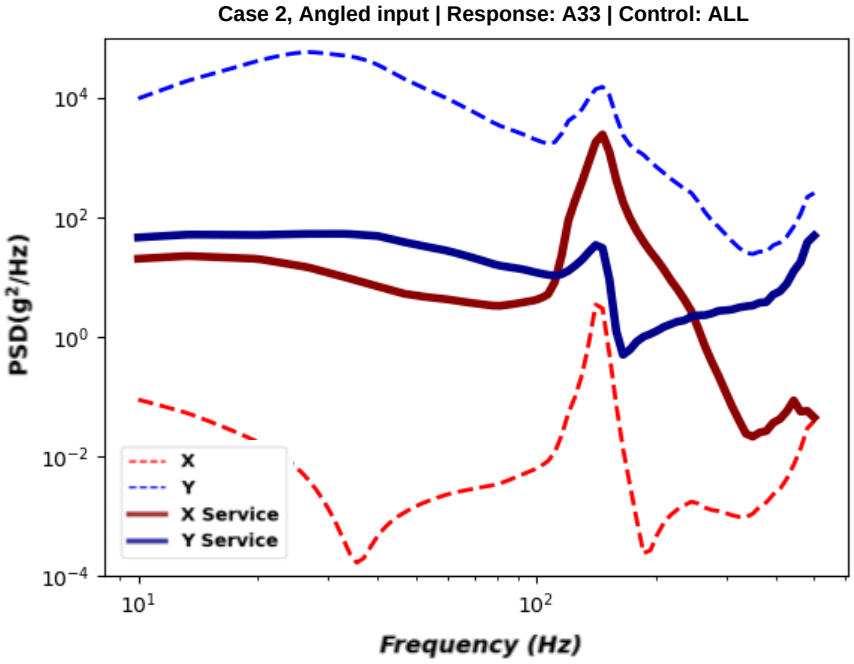

Figure 22: A33 response during Case 2 SIMO multi-axis, controlled at all locations. The dashed lines are the X and Y responses to a single, angled input. Non-optimal stiffness $k_x = 1$ and $k_y = 6.1 * 10^5\ N/m$. Optimal angle $\theta = 27°$. Resulting RMS dB error is 24.7 dB.

In Figure 22, the firmer Y springs allow the input to put more energy into the Y-axis while struggling to apply force through the very soft X springs. Even with an optimized angle, the test fixture's X-axis stiffness does not allow the input to effectively put energy into the X-axis, which ultimately leads to very dissimilar levels of the X and Y responses.

Although the relationship between the X and Y responses are similar in Figure 22 and 23, the physics causing the dissimilar responses is not the same. In Figure 23, an excitation angle of 0° means the input is entirely aligned with the test article's Y-axis. In order for an input to then excite the X-axis, it must put a large amount of energy into the Y-axis, which causes the Y response to far exceed the target.

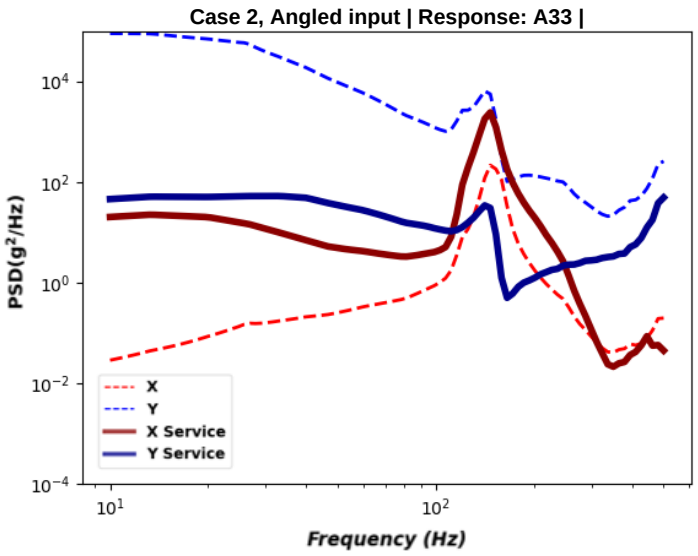

Figure 23: A33 response during Case 2 SIMO multi-axis, controlled at all locations. The dashed lines are the X and Y responses to a single, angled input. Optimal stiffness $k_x = 1.2 * 10^7$ and $k_y = 2.7 * 10^6$ N/m. Non-optimal angle $\theta = 0°$. Resulting RMS dB error is 24.3 dB.

There are positive results for the proposed method, but there is still more to do, both experimentally and in simulation, to fully validate this method.

For future simulations, a more robust optimization scheme and target

assessment method are needed. This thesis presented a simple brute force search method to search a population of stiffness combinations for a solution. We developed a few possibilities for augmenting or replacing this method with a global optimization scheme, such as simulated annealing, or with a local optimization starting from the best result of the grid search, but full assessments of these optimization approaches were out of the scope for this thesis. Likewise, the service environment/target used in this study was adequate for trialing the proposed method, but since the end goal is to produce a method which works for any given service environment, the method needs to be tested on a much larger population of service environments.

The search space for a test fixture optimization is extremely large. There are an endless number of structural optimization approaches one could try: topological optimization, layout optimization of springs, etc. In the proposed approach, the end goal of any structural optimization is to alter the mode shapes of the entire system such that the responses match the targets. For the sake of producing a tractable thesis problem, we reduced the space of all possible test fixtures down to a handful of spring parameters. Even with this simplification, there are remaining questions. It's still not clear whether the populations of stiffnesses we have searched were dense enough, or if there might be pockets of stiffness values within the population that would yield better results but were not sampled due to the coarseness of our population.

Future work is also needed to experimentally validate the method. There is work needed to determine how to physically build a parameterized test fixture. A fully robust method needs to have a test fixture which can be tuned to the required dynamics in real time, since it is uncommon for test sites to have much time with the test article before it

must be tested. The test engineer would need to be able to run a pretest and dial in the test fixture without needing to send it to a machine shop for alterations.

Finally, input modification approaches may be invaluable in supplementing the test fixture optimization. As was mentioned in the introduction, the two basic categories of research in dynamics environments testing are impedance modification and input control. Our proposed method is a novel impedance modification approach, but it may be possible to combine our approach with input control to gain further improvements. Methods utilizing dynamic substructuring could provide insights into how to optimize a shaker table input to excite the structure's modes in a way that is more representative of the service environment.

A fully validated method would enable wide access to rapid, approximate multi-axis vibration testing using existing hardware. It would eliminate the over-conservatism of sequential single-axis testing and requisite over-design of systems. This thesis presents a simulation of that method, and the results indicate that there is a strong case for pursuing it further.

REFERENCES

1. Ahlin, K. (2006). Comparison of Test Specifications and Measured Field Data. *SOUND AND VIBRATION*, 3.

2. Bendsøe, M. P., & Sigmund, O. (1999). Material interpolation schemes in topology optimization. *Archive of Applied Mechanics (Ingenieur Archive)*, *69*(9–10), 635–654. https://doi.org/10.1007/s004190050248

3. Bouma, A., Campbell, A., Roberts, T., Taylor, S., Haynes, C., & Harvey, D. (2019). Accumulated Lifetimes in Single-Axis Vibration Testing. In *Sensors and Instrumentation, Aircraft/Aerospace, Energy Harvesting & Dynamic Environments Testing, Volume 7* (Vol. 7).

4. Chandrasekhar, A., & Suresh, K. (2021). TOuNN: Topology Optimization using Neural Networks. *Structural and Multidisciplinary Optimization*, *63*(3), 1135–1149. https://doi.org/10.1007/s00158-020-02748-4

5. Daborn, P. M., Ind, P. R., & Ewins, D. J. (2014). Replicating Aerodynamic Excitation in the Laboratory. In *Topics in Modal Analysis II, Volume 7: Proceedings of the 31st IMAC, A Conference and Exposition on Structural Dynamics*.

6. Daborn, P. M., Roberts, C., Ewins, D. J., & Ind, P. R. (2014). Next-Generation Random Vibration Tests. In *Topics in Modal Analysis II, Volume 8: Proceedings of the 32nd IMAC, A Conference and Exposition on Structural Dynamics* (pp. 397–410).

7. de Silva, C. W. (2006). Vibration: Fundamentals and Practice Chapter 10. In *Vibration: Fundamentals and Practice* (2nd ed.).

8. French, R. M., Handy, R., & Cooper, H. L. (2006). A COMPARISON OF SIMULTANEOUS AND SEQUENTIAL SINGLE-AXIS DURABILITY TESTING. *Experimental Techniques*, *30*(5), 32–37. https://doi.org/10.1111/j.1747-1567.2006.00083.x

9. Gatscher, J., & Kawiecki, G. (1996). Comparison of Mechanical Impedance Methods for Vibration Simulation. In *Shock and Vibration, 3(3),* 223–232.

10. Gomez, F., & Spencer, B. F. (2019). Topology optimization framework for structures subjected to stationary stochastic dynamic loads. *Structural and Multidisciplinary Optimization*, *59*(3), 813–833. https://doi.org/10.1007/s00158-018-2103-3

11. Gregory, D., Bitsie, F., & Smallwood, D. O. (2009). Comparison of the Response of a Simple Structure to Single Axis and Multiple Axis Random Vibration Inputs. 9.

12. Hall, T. M. (2020). Analytically Investigating Impedance-Matching Test Fixtures. In *Sensors and Instrumentation, Aircraft/Aerospace, Energy Harvesting & Dynamic*

Environments Testing, Volume 7 (Vol. 7, pp. 21–31). Society of Experimental Mechanics.

13. Harvie, J. M. (2017). Using Modal Substructuring to Improve Shock & Vibration Qualification. In M. Mains & B. J. Dilworth (Eds.), *Topics in Modal Analysis & Testing, Volume 9* (pp. 227–239). Springer International Publishing. https://doi.org/10.1007/978-3-319-74700-2_24

14. Harvie, J. M., & van der Seijs, M. (2020). Application of Transfer Path Analysis Techniques to the Boundary Condition Challenge Problem. In C. Walber, P. Walter, & S. Seidlitz (Eds.), *Sensors and Instrumentation, Aircraft/Aerospace, Energy Harvesting & Dynamic Environments Testing, Volume 7* (pp. 157–166). Springer International Publishing. https://doi.org/10.1007/978-3-030-12676-6_15

15. Hoyer, S., Sohl-Dickstein, J., & Greydanus, S. (2019). Neural reparameterization improves structural optimization. *ArXiv:1909.04240 [Cs, Stat]*. http://arxiv.org/abs/1909.04240

16. Jones, R., Soine, D., Harvie, J., Schoenherr, T., Skousen, T., & Starr, M. (2018). Boundary Conditions in Environmental Testing Round Robin. 53.

17. Knight. (2020). More Representative Spacecraft Random Vibration Testing [University of Surrey]. https://doi.org/10.15126/thesis.00853129

18. Knight, C., Remedia, M., Aglietti, G. S., & Richardson, G. (2018). Satellite Vibration Testing: Angle optimisation method to Reduce Overtesting. *Acta Astronautica*, *147*, 205–218. https://doi.org/10.1016/j.actaastro.2018.04.004

19. Kolaini, A. R., Tsuha, W., & Fernandez, J. P. (2018). Spacecraft vibration testing: Benefits and potential issues. *Advances in Aircraft and Spacecraft Science*, *5*(2), 165–175. https://doi.org/10.12989/AAS.2018.5.2.165

20. Nie, Z., Lin, T., Jiang, H., and Kara, L. B. (February 3, 2021). TopologyGAN: Topology Optimization Using Generative Adversarial Networks Based on Physical Fields Over the Initial Domain. ASME. J. Mech. Des. March 2021; 143(3): 031715.

21. On, F. J. (1967). Mechanical impedance analysis for lumped parameter multi-degree of freedom/multi- dimensional systems - NASA technical reports server (NTRS). Retrieved March 13, 2023, from https://ntrs.nasa.gov/citations/19670016465.

22. Ostergaard, M. G., Ibbotson, A. R., Roux, O. L., & Prior, A. M. (2011). Virtual testing of aircraft structures. *CEAS Aeronautical Journal*, *1*(1–4), 83–103. https://doi.org/10.1007/s13272-011-0004-x

23. Qiao, Z., Weihong, Z., Jihong, Z., & Tong, G. (2012). Layout optimization of multi-component structures under static loads and random excitations. *Engineering Structures*, *43*, 120–128. https://doi.org/10.1016/j.engstruct.2012.05.013

24. Rawat, S., & Shen, M.-H. H. (2019). A novel topology optimization approach using conditional deep learning. doi:10.48550/ARXIV.1901.04859

25. Remedia, M., Aglietti, G. S., Appolloni, M., Cozzani, A., & Kiley, A. (2017). An enhanced methodology for spacecraft correlation activity using virtual testing tools. *Journal of Sound and Vibration*, *409*, 180–200. doi: 10.1016/j.jsv.2017.07.054

26. Roberts, C., & Ewins, D. (2018). Multi-axis vibration testing of an aerodynamically excited structure. *Journal of Vibration and Control*, *24*(2), 427–437. https://doi.org/10.1177/1077546316642064

27. Rohe, D. (2018). *Modal data for the BARC challenge problem Test Report*. Office of Scientific and Technical Information (OSTI).

28. Rohe, D. P., Schultz, R. A., Schoenherr, T. F., Skousen, T. J., & Jones, R. J. (2020). Comparison of Multi-Axis Testing of the BARC Structure with Varying Boundary Conditions. In C. Walber, P. Walter, & S. Seidlitz (Eds.), *Sensors and Instrumentation, Aircraft/Aerospace, Energy Harvesting & Dynamic Environments Testing, Volume 7* (pp. 179–193). Springer International Publishing. https://doi.org/10.1007/978-3-030-12676-6_17

29. Scharton, T.D. (2002). Vibration and acoustic testing of spacecraft. Sound and Vibration, 36, 14-18.

30. Scharton, T. D. (1969). *Development of impedance simulation fixtures for spacecraft vibration tests*. NASA.

31. Schoenherr, T. F. (2020). *Designing an Impedance Matched Test Fixture Using Parameterized Optimization and the Modal Projection Error.* United States.

32. Schoenherr, T. F. (2019). Derivation of Six Degree of Freedom Shaker Inputs Using Sub-structuring Techniques. In M. Mains & B. J. Dilworth (Eds.), *Topics in Modal Analysis & Testing, Volume 9* (pp. 5–14). Springer International Publishing. https://doi.org/10.1007/978-3-319-74700-2_2

33. Schoenherr, T. F., Coffin, P., & Clark, B. (2020). Use of Topology Optimization to Design Shock and Vibration Test Fixtures. In C. Walber, P. Walter, & S. Seidlitz (Eds.), *Sensors and Instrumentation, Aircraft/Aerospace, Energy Harvesting & Dynamic Environments Testing, Volume 7* (pp. 77–92). Springer International Publishing. https://doi.org/10.1007/978-3-030-12676-6_8

34. Smallwood, D. O. (2013). *The challenges of multiple input vibration testing and analysis*. 46.

35. Soine, D. E., Jones, R. J., Jr, Harvie, J. M., Skousen, T. J., & Schoenherr, T. F. (2019). Designing hardware for the boundary condition round robin challenge. In *Topics in Modal Analysis & Testing, Volume 9* (pp. 119–126). Cham: Springer International Publishing.

36. Topping, B. H. V. (Ed.). (1992). *Optimization and Artificial Intelligence in Civil and Structural Engineering*. Springer Netherlands. https://doi.org/10.1007/978-94-017-2490-6

37. Varoto, P.S., & Oliveira, L.P. (2002*). Interaction Between a Vibration Exciter and the Structure Under Test. Sound and Vibration,* 36, 20-26.

38. Waimer, S., Manzato, S., Peeters, B., Wagner, M., & Guillaume, P. (2018). Modelling and simulation of a closed-loop electrodynamic shaker and test structure model for spacecraft vibration testing. *Advances in Aircraft and Spacecraft Science*, *5*(2), 205–223. https://doi.org/10.12989/AAS.2018.5.2.205

39. Wein, F., Dunning, P. D., & Norato, J. A. (2020). A review on feature-mapping methods for structural optimization. *Structural and Multidisciplinary Optimization*, *62*(4), 1597–1638. https://doi.org/10.1007/s00158-020-02649-6

40. Yang, Y., Zhu, M., Shields, M. D., & Guest, J. K. (2017). Topology optimization of continuum structures subjected to filtered white noise stochastic excitations. *Computer Methods in Applied Mechanics and Engineering*, *324*, 438–456. https://doi.org/10.1016/j.cma.2017.06.015

41. “MIL-STD-810H, Department of Defense Test Method Standard: Environmental Engineering Considerations and Laboratory Tests.” Defense Logistics Agency, United States. 31 Jan 2019.